Available online at www.sciencedirect.com
SCIENCE DIRECT
International Journal of Heat and Fluid Flow 27 (2006) 391–401
International Journal of HEAT AND FLUID FLOW
www.elsevier.com/locate/ijhff

Comparison of zonal RANS and LES for a non-isothermal ribbed channel flow

Yan Liu [a], Paul G. Tucker [a,*], G. Lo Iacono [b]

[a] Civil and Computational Engineering Centre, School of Engineering, University of Wales, Singleton Park, Swansea SA2 8PP, UK
[b] Rothamsted Research, Harpenden, Hertfordshire AL5 2JQ, UK

Received 4 October 2004; received in revised form 17 September 2005; accepted 27 November 2005
Available online 18 January 2006

Abstract

Numerical simulations for a non-isothermal ribbed channel flow are made. Due to the relatively low Reynolds number ($Re = 14{,}200$, based on the channel height), the results have relevance to higher Reynolds number electronics cooling systems. Through considering a k–l based zonal large Eddy simulation (ZLES) method and the S–A based detached Eddy simulation (DES) approach, the predictive accuracy of hybrid methods is assessed. This is assisted through comparisons with Reynolds-averaged Navier–Stokes (RANS) model results and also measurements. The RANS models used are the zonal k–l/EASM (explicit algebraic stress model) and k–l/cubic (non-linear cubic). The k–l modelling in these is just used near walls. Comparison reveals that both ZLES and DES are capable of capturing complex unsteady flow features associated with flow separation and reattachment. In general, for the present case, ZLES and DES perform similarly and are in better agreement with measurements than results from the zonal RANS.

ZLES and DES heat transfer predictions are encouraging, the model sensitivity of results displayed when using RANS approaches being much less marked.

Keywords: Ribbed channel flow; Heat transfer; RANS; DES; LES; Electronics

1. Introduction

With ever increasing power densities, numerical simulation is now playing a key role in electronic system cooling design. According to statistics, the major factor causing electronic system failure is elevated temperatures (see Bailey, 2003). Small increases in operating temperature (of the order of 10–15 °C) can lead to a 50% reduction in the life of devices (Viswanath et al., 2000). In addition, overheated components may malfunction. Therefore, accurate prediction of flow and heat transfer in electronic systems is essential for electronics thermal design.

There are several prototype flows for electronics systems. These include channel flows with ribs or cubes mounted on a wall. Such geometries are intended to represent, to various extents, idealized circuit boards populated with integrated circuits. Numerous experimental and numerical studies have been reported in the literature on these idealized geometry flows. For example, for a fully developed ribbed channel flow, at a Reynolds number (Re) of 14,200, Acharya et al. (1993) assess flow and heat transfer predictions. The standard linear k–ϵ and Speziale's (1987) non-linear k–ϵ models are considered. Velocity and heat transfer results show that the two models perform similarly for this, essentially (in the time mean) two-dimensional (2D), flow. However, the non-linear generally improves the streamwise turbulence intensities. Iacovides and Raisee (1999) present flow and heat transfer results obtained from three low Re models for a $Re = 4 \times 10^4$, 2D, ribbed channel flow and 3D square duct flows with $Re = 5 \times 10^4$ and $Re = 1 \times 10^5$. They conclude that the use of low-Re number turbulence models is essential for heat transfer predictions, and that the Reynolds stress

* Corresponding author. Tel.: +44 1792 295255; fax: +44 1792 295598.
E-mail address: p.g.tucker@swansea.ac.uk (P.G. Tucker).

0142-727X/$ - see front matter © 2005 Elsevier Inc. All rights reserved.
doi:10.1016/j.ijheatfluidflow.2005.11.004

model yields superior heat transfer predictions to those for the linear models investigated. Bredberg and Davidson (1999) numerically explore 2D–ribbed channel flows. Relative to linear model results, the Gatski and Speziale (1993) EASM with Abid et al. (1995) damping functions is found not to improve heat transfer predictions. Bredberg et al. (2000) further illustrate that the turbulence models evaluated give predictions with an excessive Reynolds number dependency. Ooi et al. (2002) simulate heat transfer in 3D–ribbed ducts. The one-equation Spalart and Allmaras (1994) (S–A) model is found to perform better than the zonal k–l/k–ϵ (the Wolfshtein (1969) k–l model, which has less severe grid requirements, is applied near walls and the k–ϵ model in the core region), but still underpredicts heat transfer.

The turbulent periodic flow over wall-mounted cubes in a channel is obviously more complex than a ribbed channel flow (see Meinders and Hanjalić, 1999). Hence, more expensive eddy resolving modelling approaches than RANS have been employed by researchers. For example, Mathey et al. (1999) perform Smagorinsky (1963) large Eddy simulations (LES). Predictions show reasonable agreement with measurements. For the same case, Schmidt and Thiele (2002) compare the flow-field predictions for LES, detached Eddy simulation (DES) (Spalart et al., 1997) and the high-Re EASM. With DES, near walls the S–A model is used and away from them LES is implemented. Use of the former removes the need for semi-grid resolution of the near-wall streak structures in the attached flow regions. Hence, theoretically, the approach allows the use of coarser grids. Schmidt and Thiele find that the LES, requiring a finer grid, gives better predictions than the DES and EASM on a coarser grid. Zhong et al. (2003) also visit the same cube case, but using the k–l based zonal LES (ZLES) of Tucker and Davidson (2004) and Smagorinsky LES. For the ZLES, reminiscent of DES, near walls k–l RANS modelling is used. Away from walls the Yoshizawa (1993) k–l LES method is applied. The ZLES flow and heat transfer results are encouraging, being comparable in accuracy to those from LES which uses a much finer grid.

The above review suggests that RANS model performances tend to be problem dependent. Also it suggests that owing to the strong relationship between heat transfer and near-wall turbulence level, it is important to model near-wall flow behaviour accurately. In real flows, this region is also buffeted by large, geometry dependent, coherent vortices. When dealing with such features, the RANS approach generally performs poorly. Bearing in mind these points, the foregoing literature suggests that to accurately predict separated flows over complex geometries, eddy resolving schemes such as LES, ZLES and DES have potential.

Since it is a relatively low Reynolds number flow relevant to electronics and other areas of industrial application, here the ribbed channel case of Acharya et al. (1993) is revisited. The predictive abilities of ZLES and DES is explored. To aid comparison, the S–A, zonal k–l/EASM and k–l/cubic RANS models are also tested. For the latter two zonal models, the Wolfshtein (1969) k–l model is used in the near-wall regions, the Gatski and Speziale EASM (1993) and Craft et al. (1996) two-equation models being employed in the core. Use of the near-wall k–l model is attractive, reducing grid demands. Also maintaining the same simple near-wall k–l model for the RANS is helpful in discerning if there are any benefits from resolving the large eddies shed from the rib when the DES and ZLES approaches are used. Non-zonal RANS predictions for this case, using the low Reynolds number Launder–Sharma k–ϵ model and cubic model of Craft et al. (1996) can be found in Liu (2004). The current results, in the context of these simulations and the LES of Lo Iacono and Tucker (2004) will be discussed later.

2. Modelling approaches

2.1. Governing equations

For incompressible flows, the governing equations for RANS and LES can be written in the following common Cartesian coordinate weakly conservative tensor forms:

$$\frac{\partial \tilde{u}_j}{\partial x_j} = 0 \tag{1}$$

$$\rho\frac{\partial \tilde{u}_i}{\partial t} + \rho\frac{\partial\left(\tilde{u}_i\tilde{u}_j\right)}{\partial x_j} = \delta_{1j}\beta - \frac{\partial \tilde{p}}{\partial x_i} + \frac{\partial}{\partial x_j}\left[\mu\frac{\partial \tilde{u}_i}{\partial x_j}\right] - \frac{\partial \tau_{ij}}{\partial x_j} \tag{2}$$

$$\rho\frac{\partial \widetilde{T}}{\partial t} + \rho\frac{\partial\left(\tilde{u}_j\widetilde{T}\right)}{\partial x_j} = -\rho\delta_{1j}\alpha\tilde{u}_j + \frac{\partial}{\partial x_j}\left[\frac{\mu}{Pr}\frac{\partial \widetilde{T}}{\partial x_j}\right] - \frac{\partial h_j}{\partial x_j} \tag{3}$$

For RANS the tilde denotes a time- or ensemble-averaging operation. For LES it represents spatial filtering. The parameters α and β are, respectively, mean temperature and pressure gradients in the periodic streamwise direction (see Patankar et al., 1997). In Eqs. (1)–(3), $\tilde{u}_i$ is a fluid velocity component ($i = 1,2,3$ corresponding to the streamwise, wall-normal and spanwise directions, respectively); ρ, the fluid density; μ, the dynamic viscosity; $\tilde{p}$, the periodically reduced static pressure; $\widetilde{T}$, the periodic temperature; t, the time and x_j ($j = 1,2,3$), the spatial coordinate. Within the RANS context, τ_{ij} represents the Reynolds stress tensor and h_j, the turbulent heat flux tensor. For LES, τ_{ij} and h_j are the subgrid scale (SGS) stress and heat flux tensors. To obtain solutions to the above equations, the unknowns, τ_{ij} and h_j, need to be approximated.

2.2. The S–A based DES

With DES, for a normal wall distance $d \leqslant C_{\mathrm{DES}}\Delta$ ($C_{\mathrm{DES}} = 0.65$) S–A RANS modelling is used. Otherwise essentially Smagorinsky LES is implemented. Here $\Delta = \max(\Delta x, \Delta y, \Delta z)$, i.e. the maximum side length of a computational cell is taken. As can be seen, with DES the RANS/LES interface is totally grid controlled. For complex grid structures this interface (see Tucker et al., 2003) can become highly irregular.

2.3. k–l based zonal LES (ZLES)

In this study, the ZLES method of Tucker and Davidson (2004) is considered. Unlike the grid controlled DES, the interface between the Wolfshtein k–l RANS and Yoshizawa SGS model is fixed at a certain distance from walls. In this way the irregular interface problem is avoided (however, as noted later smoothing is still necessary). For the eddy viscosity based SGS models, τ_{ij} is calculated by

$$\tau_{ij} = \rho(\widetilde{u_i u_j} - \tilde{u}_i \tilde{u}_j) = \frac{\tau_{kk}}{3}\delta_{ij} - 2\mu_{\mathrm{SGS}} S_{ij} \tag{4}$$

where μ_{SGS} is the SGS eddy viscosity and the strain rate tensor $S_{ij} = (\partial\tilde{u}_i/\partial x_j + \partial\tilde{u}_j/\partial x_i)/2$. For the Yoshizawa k–l model, μ_{SGS} is obtained from

$$\mu_{\mathrm{SGS}} = \rho C_\mu l_\mu k^{1/2} \tag{5}$$

where $l_\mu = \Delta = (\Delta x \Delta y \Delta z)^{1/3}$ is the filter width and $C_\mu = 0.07$.

The SGS kinetic energy, k, is computed from the following transport equation:

$$\rho\frac{\partial k}{\partial t} + \rho\frac{\partial}{\partial x_j}(\tilde{u}_j k) = \frac{\partial}{\partial x_j}\left[(\mu + \mu_{\mathrm{SGS}})\frac{\partial k}{\partial x_j}\right] + P_k - \rho\epsilon_k \tag{6}$$

where P_k and ϵ_k are production and dissipation terms respectively, defined as

$$P_k = 2\mu_{\mathrm{SGS}} S_{ij} S_{ij}, \quad \epsilon_k = C_\epsilon \frac{k^{1.5}}{l_\epsilon} \tag{7}$$

In the above, $C_\epsilon = 1.05$ and $l_\epsilon = \Delta$. In the RANS zone, l_μ and l_ϵ use the expressions of Wolfshtein (1969). Also, the constants of Wolfshtein are used in this zone.

To deal with the significant change of turbulent viscosity caused by specifying the RANS/LES interface, a number of proposals have been advocated in the literature (Tucker and Davidson, 2004; Temmerman et al., 2003). In this work, Tucker and Davidson's (2004) multigrid restriction operator based numerical smoothing of modelled turbulence length scales is applied.

2.4. RANS modelling

In addition to the S–A model, the EASM and cubic non-linear RANS models are implemented in zonal forms. As mentioned in the introduction, near walls the economical linear k–l model is used. Away from them, the EASM and cubic are employed. The modelled Reynolds stresses, $\tau_{ij} = \rho\widetilde{u_i' u_j'}$ (in which the primes represent fluctuating components), consist of linear and non-linear parts. All the RANS models investigated are well detailed in the references given in the introduction and so these relatively standard details are not repeated here. The interface between the k–l and either the EASM or cubic model is set at $y^*_{\mathrm{int}} = 60$ (the dimensionless wall distance $y^* = \rho y C_\mu^{1/4} k^{1/2}/\mu$). Fuller zonal modelling details can be found in Liu (2004).

2.5. Thermal modelling

For both RANS and LES computations, the following simple eddy diffusivity model is used:

$$h_j = -\frac{\mu_T}{Pr_{\mathrm{t}}}\frac{\partial\widetilde{T}}{\partial x_j} \tag{8}$$

For RANS, $\mu_{\mathrm{T}} = \mu_{\mathrm{t}}$ (turbulent or eddy viscosity) and the turbulent Prandtl number $Pr_{\mathrm{t}} = 0.9$. In LES zones, $\mu_{\mathrm{T}} = \mu_{\mathrm{SGS}}$ and $Pr_{\mathrm{t}} = 0.4$ (see Tucker and Davidson, 2004). By substituting Eq. (8) into Eq. (3), the following diffusion coefficient or thermal diffusivity can be obtained:

$$\Gamma = \frac{\mu}{Pr} + \frac{\mu_{\mathrm{T}}}{Pr_{\mathrm{t}}} \tag{9}$$

For a constant heat flux imposed along a wall, q''_{w}, the local Nusselt number is defined as

$$Nu = \frac{q''_{\mathrm{w}} D_{\mathrm{h}}}{k(T_{\mathrm{w}}(x) - T_{\mathrm{b}}(x))} \tag{10}$$

where $k = \mu c_p/Pr$ is thermal conductivity. In the above, $T_{\mathrm{w}}(x)$ and $T_{\mathrm{b}}(x)$ are the wall and bulk (in the y–z plane) temperatures at x, respectively. The hydraulic diameter of the channel is D_{h}.

2.6. Configuration studied, boundary conditions and numerical details

Fig. 1 shows a schematic of the ribbed channel configuration under study. Flow parameters consistent with the measurements of Acharya et al. (1993) are summarized in Table 1. The Reynolds number, Re, is based on the channel height (H) and mean (or bulk) velocity (U_0). Note, since the channel width is finite, $D_{\mathrm{h}} \neq H$. In the streamwise (x) and spanwise (z) directions, periodic boundary conditions are applied for both the flow field and temperature. Periodicity was explicitly added to the solver, a cyclic TDMA algorithm (Patankar et al., 1997) being used in the z direction and periodic Gauss–Siedel algorithm in the x. At walls, for velocities, the usual no slip and impermeability condi-

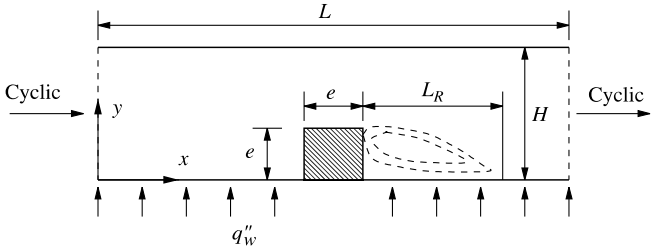

Fig. 1. Schematic of the ribbed channel configuration.

Table 1
Flow parameters for the ribbed channel flow

Re	L	H	U_0	e	D_{h}	q''_{w}
14,200	0.127 m	0.061 m	3.6 m/s	0.00635 m	0.1016 m	280 W/m^2

tions are used. Constant heat flux is imposed along the bottom wall. On the rib surface and top channel wall, an adiabatic boundary condition is applied.

To drive the flow a source term was used in the streamwise momentum equation (see Eq. (2)). The magnitude of this was adjusted to match the desired Reynolds number. Also, a source term was used in the energy equation (see Eq. (3)). The mean pressure, β, and mean temperature, α, gradients are calculated respectively from the following equations:

$$\beta_{\text{new}} = \beta_{\text{old}} - \rho\left(\frac{(Q_{\text{new}} - Q_0) - 0.5(Q_{\text{old}} - Q_0)}{0.5\,\Delta t H z_{\max}}\right) \tag{11}$$

$$\alpha = \frac{q''_{\text{w}}}{\rho c_p H U_0} \tag{12}$$

The subscripts, 'new' and 'old' in the above, refer to the new and old time levels, respectively. Q_0 is the specified volume flow rate and the product $Hz_{\max}$ gives the channel cross-sectional area.

Regarding grid generation, attention is paid to the separated flow and boundary layer regions. A two-parameter tanh function is used to stretch the grid. A geometric expansion is employed in the y direction. For the eddy resolving approaches the grid is uniform in the z direction.

For 2D RANS simulations a 199×142 (x, y) grid is used. For DES, ZLES and LES, 3D simulations are carried out. A mesh with $121 \times 112 \times 33$ (x, y, z) nodes is employed along with one where the number of z nodes is doubled. Also, Smagorinsky LES results of Lo Iacono and Tucker (2004) for a finer grid with $215 \times 215 \times 105$ nodes are considered. It is worth noting that the extra nodes used for the RANS simulations are unnecessary, the number of grid nodes used for the ZLES and DES being sufficient for sensibility of grid independent RANS results. For the 3D computations, the domain width is $9.5e$. The non-dimensional mesh distributions (normalized by L or H) for the ZLES/DES are shown in Fig. 2 (note here $\mathrm{d}x = \Delta x$ and $\mathrm{d}y = \Delta y$). A posteriori study on this mesh, based on local wall shear stress, shows that at first off-wall grid nodes $y^+ \approx 1$. Also, for the lower wall, the streamwise Δx^+ and spanwise Δz^+ (for 33 cross-stream nodes) vary between 1 and 35, the average values being 15 and 23, respectively.

For ZLES, because of the significantly different values of Pr_{t} in the RANS and LES regions, the harmonic mean for Pr_{t} is used when discretizing Eq. (3). At control-volume faces, which for the current cell vertex scheme are located exactly halfway between node points, e.g. i, j, k and i, $j+1$, k, the diffusion coefficient takes the following form:

$$\Gamma = \frac{2\Gamma_{i,j,k}\Gamma_{i,j+1,k}}{\Gamma_{i,j,k} + \Gamma_{i,j+1,k}} \tag{13}$$

Similar expressions can be obtained for Γ at other faces. As noted earlier, to smooth ZLES length scales, multigrid restriction operators are used. Following Tucker and Davidson (2004), the interface (y_{int}) of the RANS and LES regions is tested at 10% and also 20% of the rib height

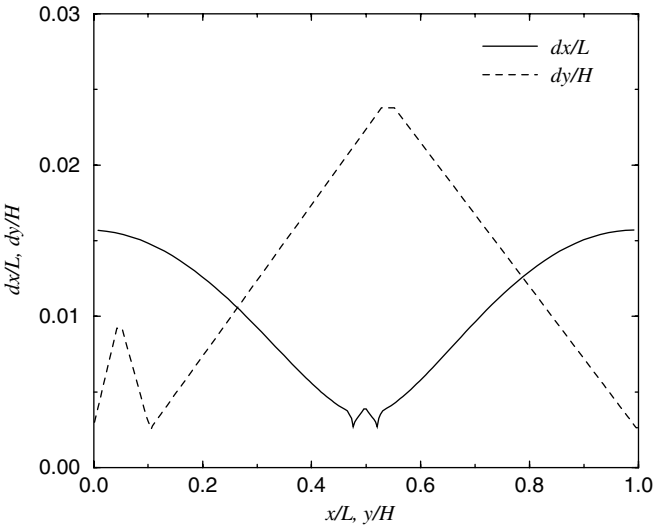

Fig. 2. Variation of grid spacings in the x and y directions.

(e). The alternative would be to base the interface on y^* or y^+. But due to the highly separated, low Reynolds number nature of the current flow this becomes less appropriate. For the current grid, in the DES computation, the interface between RANS and LES is located at 16–18%e from walls.

A finite volume based solver (Tucker, 2001) is employed. For spatial discretization, second-order central differences are used. For temporal terms, the Crank–Nicolson scheme is used for LES and hybrid RANS/LES simulations and a first-order fully implicit scheme for RANS. Ensuring good energy conservation properties, which can be important for the LES, velocity grid nodes are staggered relative to the pressure nodes. For pressure–velocity coupling, the SIMPLE algorithm of Patankar and Spalding (1972) is applied.

3. Results and discussion

It should be noted that, unless otherwise stated, the ZLES and DES results in this section use the coarser cross-stream grid, profiles for the two grids being remarkably similar.

3.1. Flow structure

Instantaneous streamlines at mid x–y plane from the coarse grid LES, ZLES and DES are shown in Fig. 3. Frame (d) gives a zoomed in view around the rib region for the LES. Observation of other instantaneous flow fields (not shown here) demonstrates that, as would be expected, for these eddy resolving approaches, near the rib, the flow varies significantly over time with large scale eddies being shed downstream of the rib. However, away from the rib for $y/H > 0.45$, the flow appears almost steady/laminar. The RANS yields steady-state results.

Time-averaged streamlines for the ZLES, DES, LES and S–A model are presented in Fig. 4. As can be seen from these plots, all simulations exhibit the same general broad

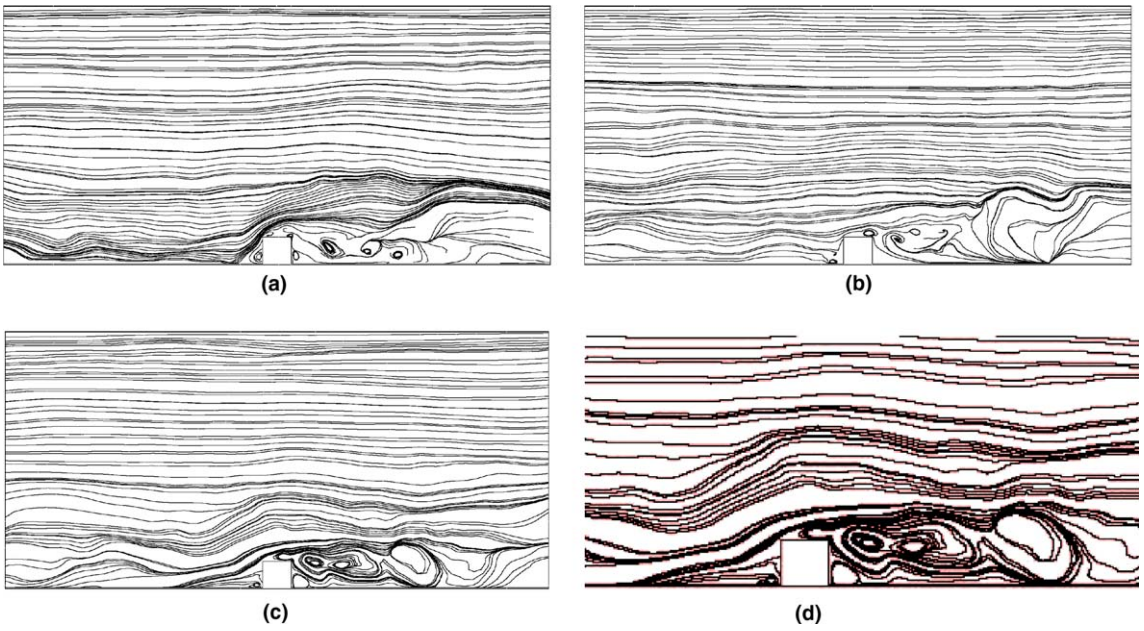

Fig. 3. Mid x–y plane instantaneous streamlines: from (a) ZLES, (b) DES, (c) LES and (d) zoom-in of (c).

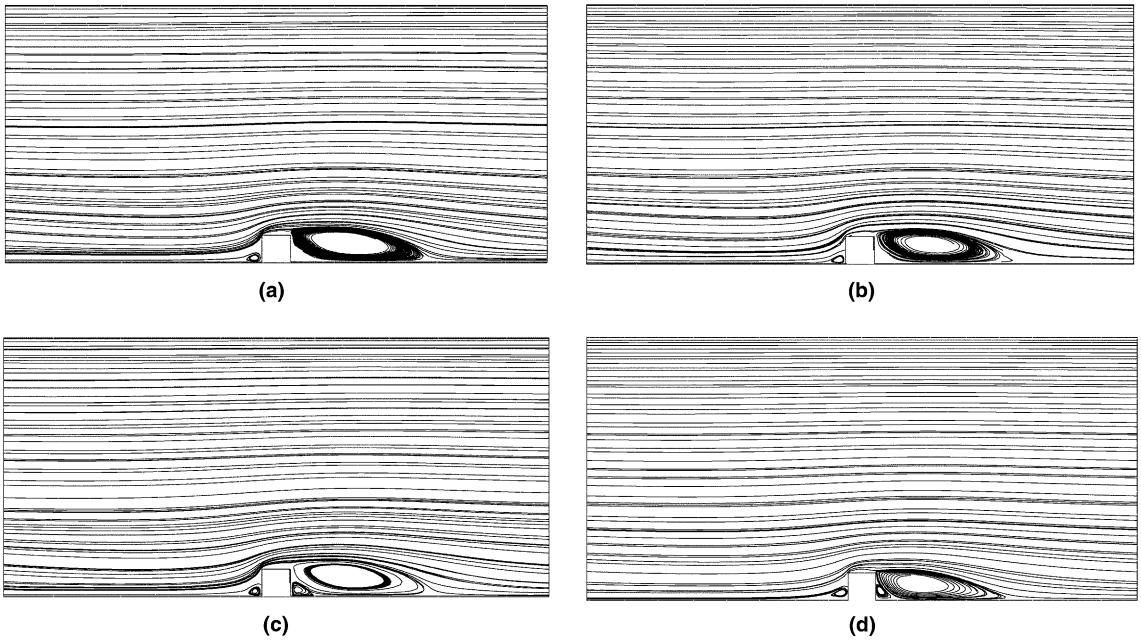

Fig. 4. Mid x–y plane time-averaged streamlines: from ZLES (a), DES (b), Smagorinsky LES (c) and S–A (d).

flow features. These include flow impingement and a small recirculation region (of the scale $e/3$) at the rib front face. Downstream of the rib, the flow separates with a further larger recirculation region generated. The k–l/EASM and k–l/cubic models generate similar flow patterns to the S–A model.

Fig. 5 shows instantaneous y–z plane streamlines for the ZLES. Frames (a, b) are for 33 z direction nodes, while frames (c, d) are for 67. Also, frames (a) and (c) are at $x/L = 0.5$ and frames (b) and (d) at $x/L = 0.6$. As would be expected, the finer grid supports smaller flow structures. However, both support significant levels of flow three-dimensionality and mean velocity and stress distributions for the two grids are very similar (not shown here). Clearly, 33 grid nodes in the z direction are too few to resolve structures of the scale of the rib. Nevertheless, unexpectedly, this does not seem to matter for accurate prediction of the data given by Acharya et al. (1993).

The predicted-dimensionless reattachment lengths, L_R (see Fig. 1), are summarized in Table 2. The measurement gives $L_R/e = 6 \pm 0.7$. As can be seen, except for the k–l/EASM, which significantly overpredicts L_R/e, the other

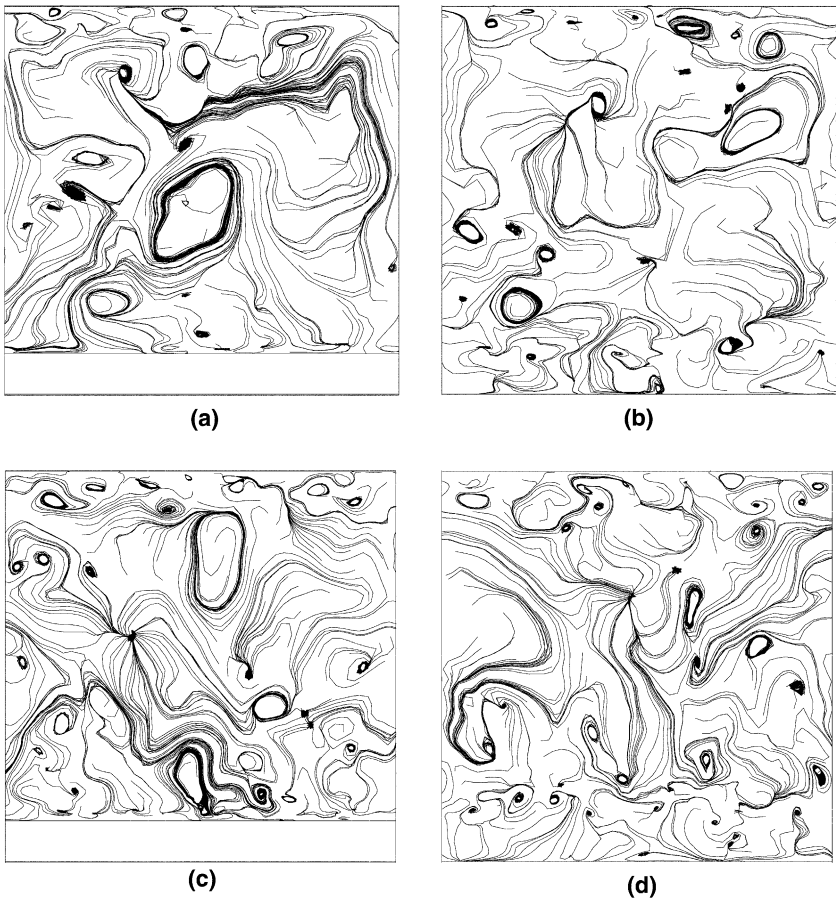

Fig. 5. Instantaneous y–z plane streamlines for ZLES: (a, b) coarser grid ZLES; (c, d) finer grid ZLES ((a, c) at $x/L = 0.5$; (b, d) at $x/L = 0.6$).

Table 2
Predicted dimensionless reattachment length

Model	Measurement	LES	ZLES	DES	S–A	k–l/EASM	k–l/cubic
L_R/e	6 ± 0.7	5.6	5.5	5.9	5.7	8.1	6.4

results are within the measurement uncertainty. It is worth noting that in Bredberg and Davidson (1999), the low Re EASM also overpredicts L_R for a similar case.

3.2. Mean velocity distributions

Fig. 6 shows the normalized mean streamwise velocity, U, profiles obtained from the ZLES and DES at the following seven axial locations: $x/e = 2.3$, 10, 10.5, 11.1, 13.6, 16.2 and 17.6. It should be mentioned that $x/e = 10$ and 10.5 correspond to the centre and right edge of the rib, respectively. Except for one location at $x/e = 2.3$ which is upstream of the rib, the others are situated downstream of the rib. From the plots, it can be seen that the ZLES and DES perform similarly, with the DES giving slightly lower U predictions. In the core region, the predictions agree well with the measurements. In the near-wall regions, immediately above the rib, and downstream of the rib, both models underpredict U. Fig. 7 repeats Fig. 6 but this time for the following RANS models: S–A, k–l/cubic and k–l/EASM. These generally yield similar encouraging results. However, in the recirculation region, the k–l/EASM significantly underpredicts U. This leads to the overprediction of L_R/e. Comparing Figs. 6 and 7 shows for $y/e < 2$ the ZLES and DES give slightly lower U predictions than the RANS. Figs. 8 and 9 show that for V, both the ZLES and DES are generally more accurate than the RANS. However, in the recirculation region all models underpredict V.

3.3. High-order statistics

Figs. 10 and 12 show resolved turbulent normal stresses for the ZLES and DES. Figs. 11 and 13 are the equivalent plots to Figs. 10 and 12 but for the RANS. Fig. 14 contrasts shear-stress components for the ZLES, DES and RANS models.

The measured $\overline{u'u'}^{1/2}$ profiles between $x/e = 10$ and $x/e = 11.1$ show peaks. These arise from shear-layer turbulence generation at the rib top surface. As the flow moves downstream, these decrease. In comparison with the RANS predictions (Fig. 11), both the ZLES and DES (Fig. 10) capture the peaks better than the RANS. However, in the rib proximity they still underpredict them. Upstream and downstream of the rib, the ZLES and

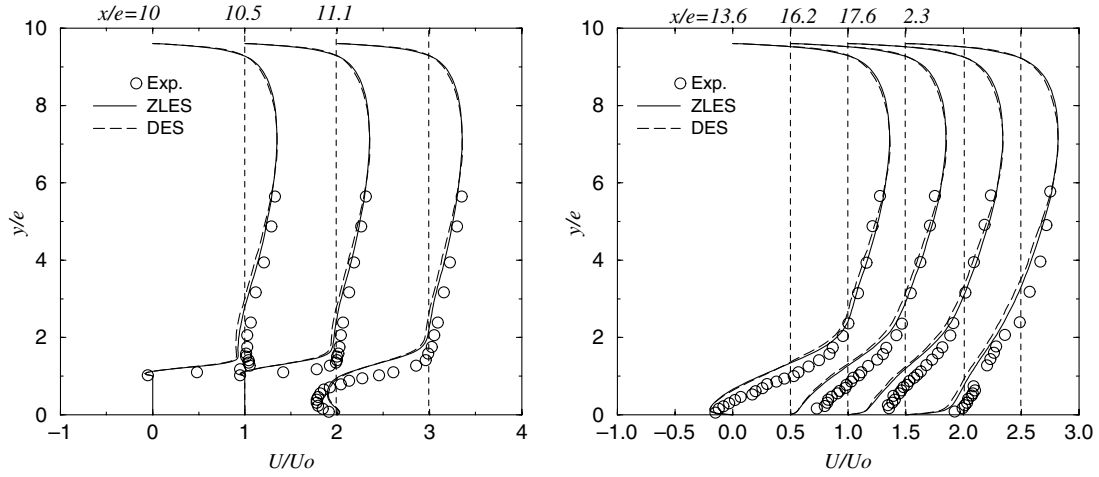

Fig. 6. Variation of the streamwise velocity with y at seven axial locations for ZLES and DES.

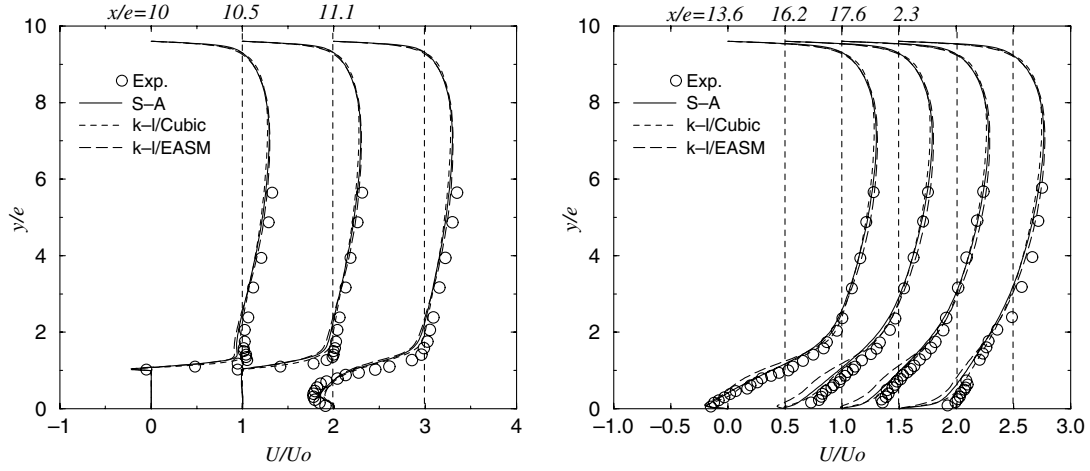

Fig. 7. Variation of the streamwise velocity with y at seven axial locations for RANS models.

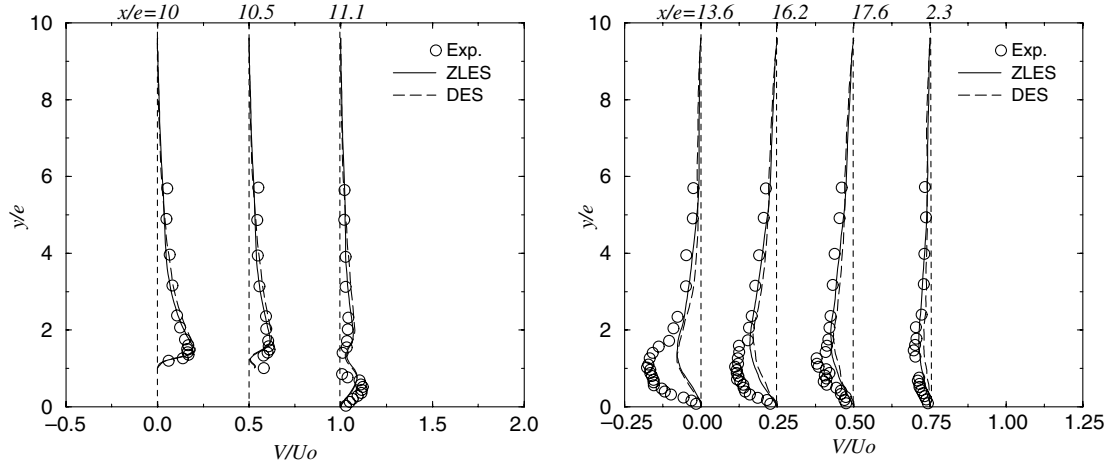

Fig. 8. Variation of the cross-stream velocity with y for ZLES and DES.

DES show encouraging agreement with the measurements, the DES giving slightly larger $\overline{u'u'}^{1/2}$ predictions. The zonal k–l/cubic model (see Fig. 11) performs slightly better than the k–l/EASM.

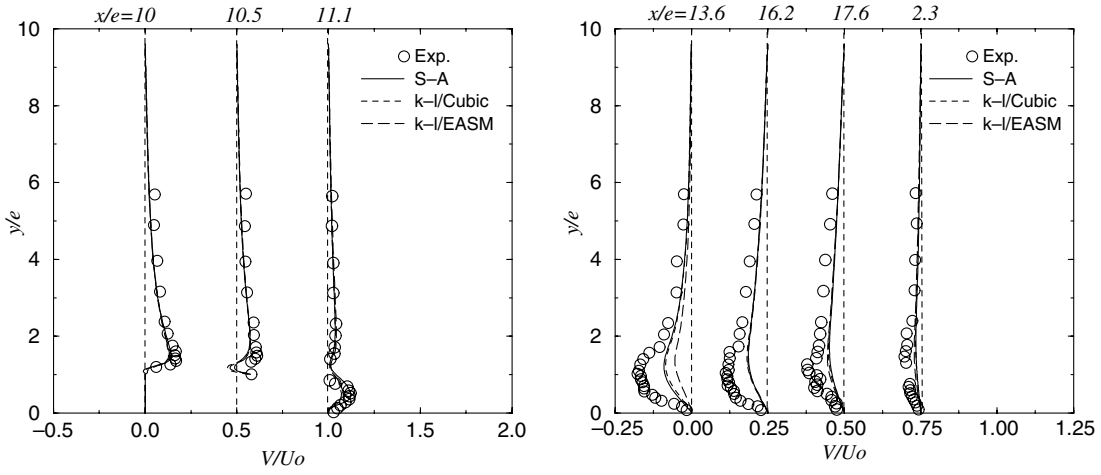

Fig. 9. Variation of the cross-stream velocity with y for RANS models.

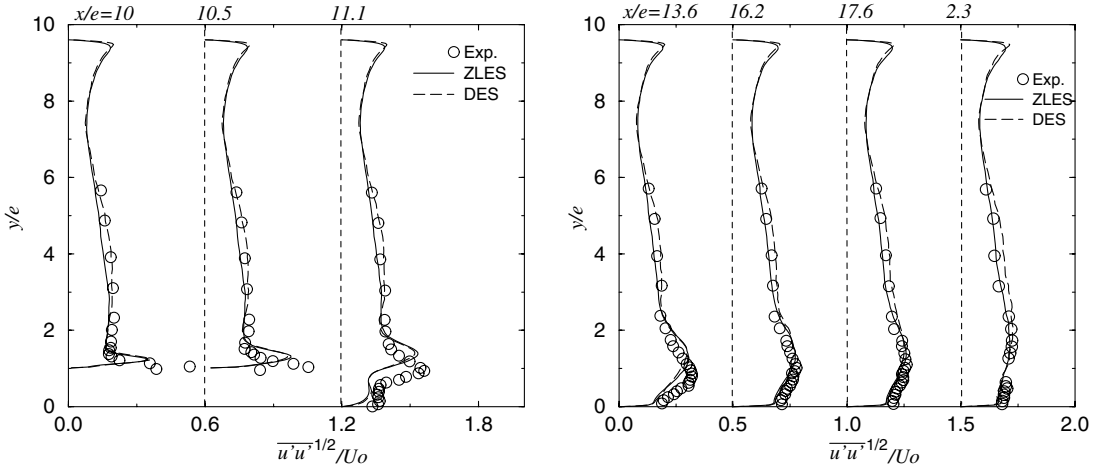

Fig. 10. Variation of the streamwise velocity fluctuation with y for ZLES and DES.

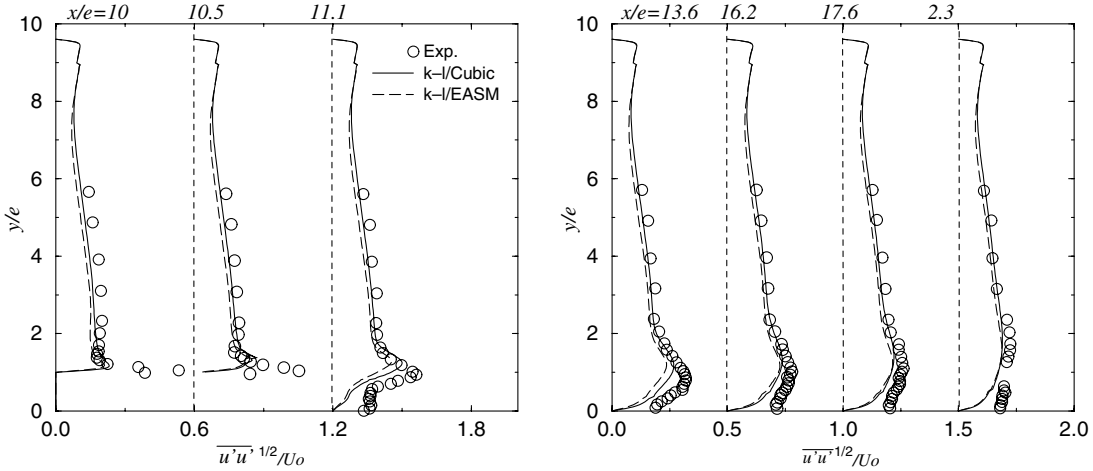

Fig. 11. Variation of the streamwise velocity fluctuation for RANS models.

Figs. 12 and 13 show that generally, in the core region, all models predict $\overline{v'v'}^{1/2}$ well. However, for $10 \leqslant x/e \leqslant 11.1$ the k–l/cubic slightly overpredicts $\overline{v'v'}^{1/2}$. In the near-wall region, the RANS simulations perform marginally better than the ZLES and DES. It is expected that when using a finer grid (or high-order discretization) for the ZLES and DES, this difference would reduce. Some profiles show a kink. These correspond to the interface between the dif-

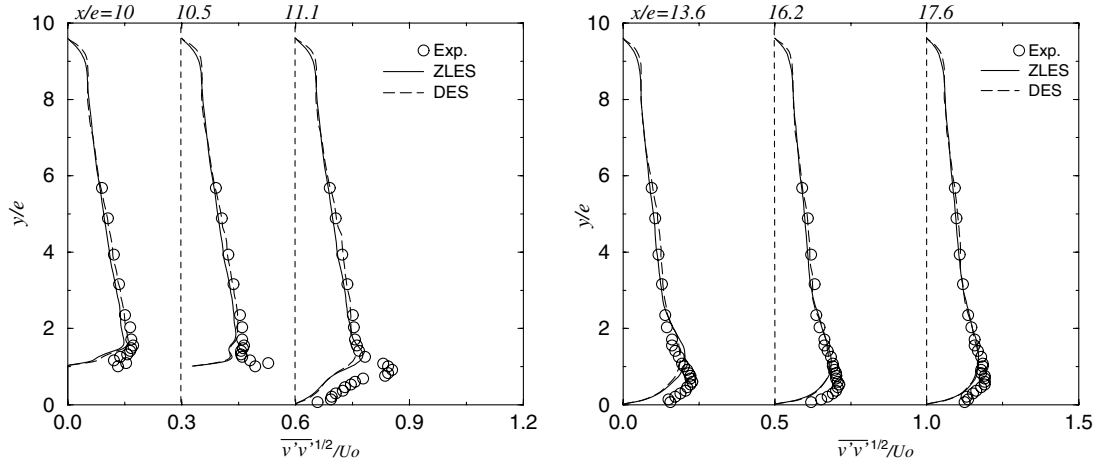

Fig. 12. Variation of the cross-stream velocity fluctuation for ZLES and DES.

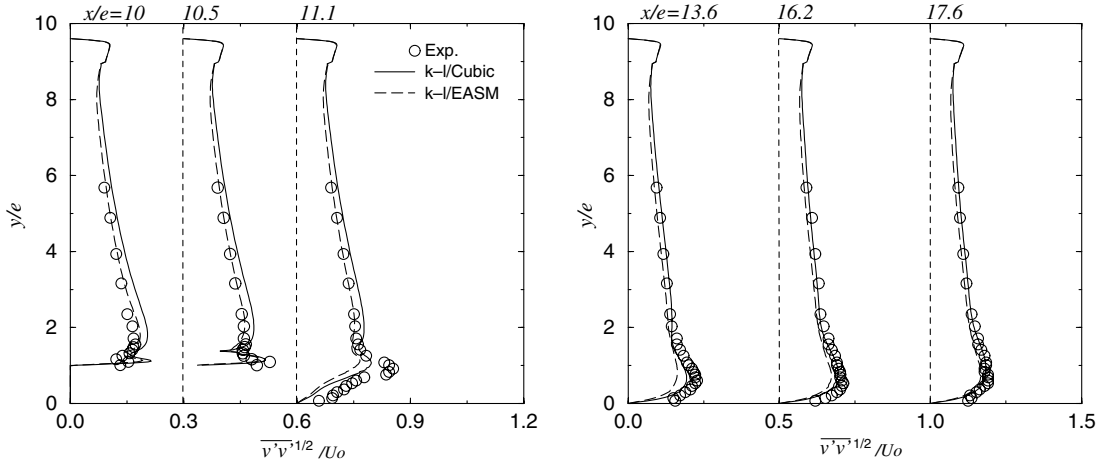

Fig. 13. Variation of the cross-stream velocity fluctuation for RANS models.

fering turbulence models. It is well known that the S–A model does not predict $\overline{u'u'}$ and $\overline{v'v'}$ well. Therefore, Figs. 11 and 13 omit this data.

Fig. 14 gives normalized shear stress distributions. Frame (a) gives the ZLES and DES results and (b) the RANS. As can be seen, as with the normal stresses, all

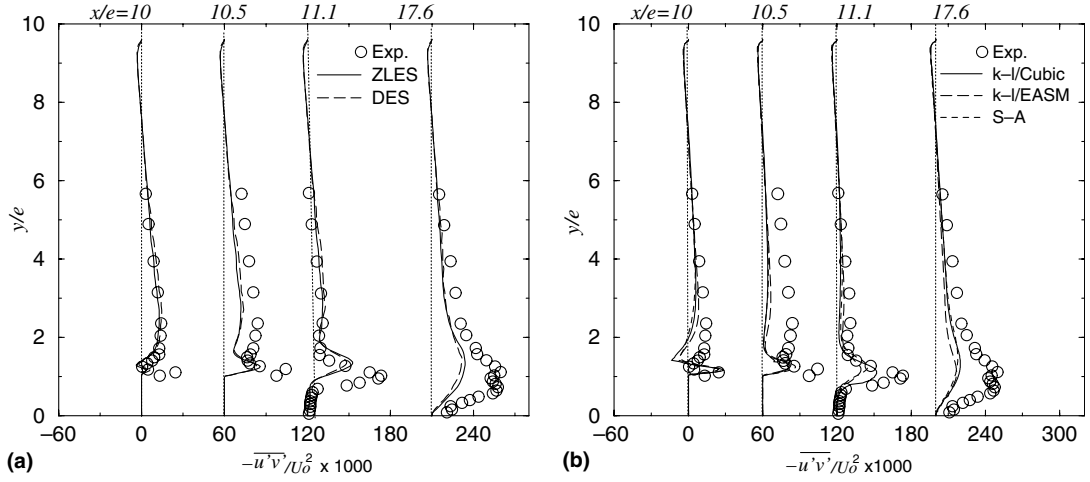

Fig. 14. Normalized shear stress distributions at four locations: (a) ZLES and DES and (b) RANS models.

models fail to predict the magnitude of the peaks in $\overline{u'v'}$. In general, the ZLES and DES results are in slightly better agreement with the measurements than the RANS.

Comparisons (not given in the plots) show the present ZLES and DES perform considerably (especially upstream and downstream of the wake region where wall modelling becomes more important) better than the fine grid LES data of Lo Iacono and Tucker (2004) and also the pure Smagorinsky LES for the same grid as used here.

3.4. Heat transfer results

Fig. 15 compares the predicted and measured *Nu* distributions. As can be seen, like the measurements, all the predicted *Nu* distributions have two peaks associated with impingement ($x/e = 9.5$) and reattachment ($x/e \approx 16$). However, the location of these is model dependent. Fig. 15 shows the ZLES and DES produce similar *Nu* results, both giving satisfactory predictions upstream of the rib. However, prior to reattachment, both methods underpredict *Nu*. After reattachment, the ZLES overpredicts *Nu*, while the DES *Nu* matches the measurements well. For such a simple turbulence model, the S–A predicts *Nu* remarkably accurately. However, it is worth noting that as far as wall heat transfer is concerned, the S–A model is not that much simpler than the other RANS models. This is because in the crucial near-wall regions they are all reduced to one-equation models. The *k–l*/cubic model yields better *Nu* predictions than the *k–l*/EASM. Owing to the velocity underprediction (see Fig. 7), the latter also largely underpredicts *Nu*. It is also worth noting that underprediction of heat transfer in recirculation zones is typical of *k–l* based zonal models (see, for example, Ooi et al., 2002). It should be mentioned that the low Reynolds number Launder–Sharma k–ϵ and cubic model predictions in Liu (2004) show a similar error level but this time overpredicting heat transfer.

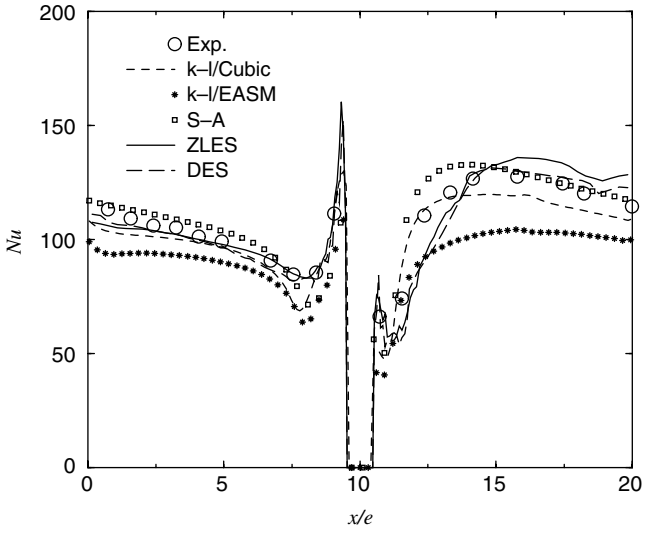

Fig. 15. Local Nusselt number distributions.

Table 3
Predicted dimensionless maximum *Nu* locations

Model	Measurement	LES	ZLES	DES	S–A	*k–l*/EASM	*k–l*/cubic
x/e	15.6 ± 0.4	16.0	15.8	14.8	14.0	14.8	15.8

The maximum measured Nusselt number (Nu_{max}) is upstream of the reattachment point (at $x/e = 16.5 \pm 0.7$) at $x/e = 15.6 \pm 0.4$. Table 3 summarizes the predicted maximum *Nu* locations (for $x/e > 10$) from the models. It shows that the Nu_{max} location predicted from the S–A model occurs too far upstream at $x/e = 14$, followed by the *k–l*/EASM and DES. The others predict Nu_{max} within the experimental uncertainty. Note, the data in Lo Iacono and Tucker (2004) is isothermal and hence Table 3 LES Nu_{max} value is obtained from the pure LES based on the coarse grid.

The above ZLES data is for $y_{int} = 10\%e$. ZLES results for $y_{int} = 20\%e$ (not shown here) are generally less satisfactory, giving for example around 10% lower predictions for velocities. This is understandable because in the zonal context the LES zone diminishes and RANS region rises with increasing y_{int}. This means that less eddies are resolved and more modelled.

4. Conclusions

RANS and hybrid RANS/LES approaches were used to simulate the flow and heat transfer in a ribbed channel. For the flow field, generally, ZLES and DES gave similar pleasing results. For RANS, the S–A, *k–l*/cubic and *k–l*/EASM models yielded satisfactory mean velocities. However, in the recirculation region the *k–l*/EASM underpredicted velocities. Except for the *k–l*/EASM, all other models predicted a reasonable (<8% error) reattachment length. Generally, as expected, in terms of flow structure, mean velocities and their fluctuations, both the ZLES and DES marginally improved the flow field prediction. For ZLES, when increasing y_{int} by 10% of e, the results get worse. Since the RANS extent increases and LES decreases, this is not surprising.

Comparisons of heat transfer results showed that the ZLES and DES predicted the correct *Nu* trend and matched the measurements satisfactorily. Considering its simplicity away from walls, the S–A model gave impressive heat transfer results. The *k–l*/cubic model performed better than the *k–l*/EASM. However, except for the S–A model, all other RANS results underpredicted heat transfer. Importantly, predicted RANS heat transfer levels are more strongly dependent on model choice than the ZLES and DES.

References

Acharya, S., Dutta, S., Myrum, T.A., Baker, R.S., 1993. Periodically developed flow and heat transfer in a ribbed duct. Int. J. Heat Mass Transfer 36 (8), 2069–2082.

Abid, R., Rumsey, C., Gatski, T.B., 1995. Prediction of nonequilibrium turbulent flows with explicit algebraic stress model. AIAA J. 33, 2026–2031.

Bailey, C., 2003. Modelling the effect of temperature on product reliability. In: 19th IEEE SEMI-THERM Symposium, San Jose, CA, pp. 324–331.

Bredberg, J., Davidson, L., 1999. Prediction of flow and heat transfer in a stationary two-dimensional rib roughened passage using low-*Re* turbulent models. In: 3rd European Conference on Turbomachinery, IMech., pp. 963–972.

Bredberg, J., Davidson, L., Iacovides, H., 2000. Comparison of near-wall behavior and its effect on heat transfer for k–ω and k–ϵ turbulence models in rib-roughened 2D channels. In: Nagano, Y., Hanjalic, K., Tsuji, T. (Eds.), 3rd International Symposium on Turbulence, Heat and Mass Transfer, Aichi Shuppan, pp. 381–388.

Craft, T.J., Launder, B.E., Suga, K., 1996. Development and application of a cubic eddy-viscosity model of turbulence. Int. J. Heat Fluid Flow 17 (2), 108–115.

Gatski, T.B., Speziale, C.G., 1993. On explicit algebraic stress models for complex turbulent flows. J. Fluid Mech. 254, 59–78.

Iacovides, H., Raisee, M., 1999. Recent progress in the computation of flow and heat transfer in internal cooling passages of turbine blades. Int. J. Heat Fluid Flow 20, 320–328.

Liu, Y., 2004. Numerical simulations of unsteady complex geometry flows. Ph.D. thesis. School of Engineering, University of Warwick, UK.

Lo Iacono, G., Tucker, P.G., 2004. LES computation of partial transport in rib roughened passages. In: Proceedings of the CHT-04 ICHMT International Symposium on Advances in Computational Heat Transfer, Norway, CHT-04-103.

Mathey, F., Fröhlich, J., Rodi, W., 1999. LES of heat transfer in turbulent flow over a wall-mounted matrix of cubes. In: Proceedings of Workshop on Direct and Large Eddy Simulation, Isaac Newton Institute Cambridge, Kluwer Academic, pp. 51–62.

Meinders, E.R., Hanjalić, K., 1999. Vortex structure and heat transfer in turbulent flow over a wall-mounted matrix of cubes. Int. J. Heat Fluid Flow 20, 255–267.

Ooi, A., Iaccarino, G., Durbin, P.A., Behnia, M., 2002. Reynolds averaged simulation of flow and heat transfer in ribbed ducts. Int. J. Heat Fluid Flow 23, 750–757.

Patankar, S.V., Liu, C.H., Sparrow, E.M., 1997. Fully developed flow and heat transfer in ducts having streamwise-periodic variations of cross-sectional area. ASME J. Heat Transfer 99, 180–186.

Patankar, S.V., Spalding, D.B., 1972. A calculation procedure for heat, mass and momentum transfer in three-dimensional parabolic flows. Int. J. Heat Mass Transfer 15, 1787–1806.

Schmidt, S., Thiele, F., 2002. Comparison of numerical methods applied to the flow over wall-mounted cubes. Int. J. Heat Fluid Flow 23, 330–339.

Smagorinsky, J., 1963. General circulation experiments with the primitive equations. I. The basic experiment. Month. Weath. Rev. 91, 99–165.

Spalart, P.R., Allmaras, S.R., 1994. A one-equation turbulence model for aerodynamic flow. La Recherche Aerospatiale 1, 5–21.

Spalart, P.R., Jou, W.H., Strelets, M., Allmaras, S.R., 1997. Comments on the feasibility of LES for wings, and on a hybrid RANS/LES approach. In: First AFOSR International Conference on DNS/LES in Advances in DNS/LES, pp. 137–147.

Speziale, C.G., 1987. On non-linear k–l and k–ϵ models of turbulence. J. Fluid Mech. 178, 459–475.

Temmerman, L., Leschziner, M.A., Hanjalić, K., 2003. A combined RANS-LES strategy with arbitrary interface location for near-wall flows. In: Kasagi, N., Eaton, J.K., Friedrich, R., Humphrey, J.A.C., Leschziner, M.A., Miyauchi, T. (Eds.), Proceedings of the 3rd International Symposium on Turbulence and Shear Flow Phenomena, Sendai, Japan, pp. 929–934.

Tucker, P.G., 2001. Computation of Unsteady Internal Flows. Kluwer Academic Publisher, Dordrecht.

Tucker, P.G., Davidson, L., 2004. Zonal k–l based large eddy simulations. Computers and Fluids 33, 267–287.

Tucker, P.G., Davidson, L., Liu, Y., 2003. Hybrid k–l based large eddy simulation modelling. In: Hanjalić, K., Nagano, Y., Tummers, M.J. (Eds.), 4th International Symposium on Turbulence, Heat and Mass Transfer, pp. 681–688.

Viswanath, R., Wakharkar, V., Watwe, A., Lebonheur, V., 2000. Thermal performance challenges from silicon to system. Intel Technology Journal Q3, 1–16.

Wolfshtein, M., 1969. The velocity and temperature distribution in one-dimensional flow with turbulence augmentation and pressure gradient. Int. J. Heat Mass Transfer 12, 301–318.

Yoshizawa, A., 1993. Bridging between eddy-viscosity-type and second-order models using a two-scale DIA. In: Proceedings of the 9th International Symposium on Turbulent Shear Flow, Kyoto, 23.1.1-6.

Zhong, B., Tucker, P.G., Liu, Y., 2003. On a hybrid LES/RANS approach and its application to flow over a matrix of surface mounted cubes. In: Hanjalić, K., Nagano, Y., Tummers, M.J. (Eds.), 4th International Symposium on Turbulence, Heat and Mass Transfer, Antalya, Turkey, pp. 705–712.